Rare Metal Materials and Engineering
Volume 54, Issue 12, December 2025
Available online at www.rmme.ac.cn

Science Press

Cite this article as: Shi Changgen, Jiang Jialin, Wang Haitao, et al. Numerical Simulation and Experiment of TA1/Q235 Composite Plate by Explosive Welding[J]. Rare Metal Materials and Engineering, 2025, 54(12): 3032-3047. DOI: https://doi.org/10.12442/j.issn.1002-185X.20240670.

ARTICLE

Numerical Simulation and Experiment of TA1/Q235 Composite Plate by Explosive Welding

Shi Changgen, Jiang Jialin, Wang Haitao, Luo Xuchuan, Feng Ke

Army Engineering University of PLA, Nanjing 210007, China

Abstract: To further reduce the explosive thickness and to improve the bonding quality of titanium/steel composite plates, explosive welding experiments of TA1/Q235 were conducted using a low detonation velocity explosive (53#) under the guidance of the explosive welding lower limit principle with the flyer plate thicknesses of 1, 2, and 4 mm and gaps of 3, 6, and 8 mm. The weldability window for titanium/steel explosive welding was calculated, and a quantitative relationship between dynamic and static process parameters was developed. A β-V_p high-speed inclined collision model was proposed, and two-dimensional numerical simulations for the explosive welding tests were performed using the smoothed particle hydrodynamics (SPH) algorithm, revealing the growth evolution mechanisms of the typical waveform morphology characteristics. Through microstructural characterization techniques, such as optical microscope, scanning electron microscope, energy dispersive spectrometer, and electron backscattered diffractometer, and mechanical property tests in terms of shear strength, bending performance, and impact toughness, the microstructure and mechanical properties of the interfaces of explosively welded TA1/Q235 composite plates were investigated. Results show that the quality of interface bonding is excellent, presenting typical waveform morphology with an average interface shear strength above 330 MPa and an average impact toughness exceeding 81 J. All samples can be bent to 180° without significant delamination or cracking defects.

Key words: explosive welding; weldability window; SPH numerical simulation; microstructure; mechanical property

1 Introduction

Titanium/steel composite plates have combined advantages of different materials, such as the excellent corrosion resistance and high specific strength of titanium as well as the high strength and low cost of steel. Their traditional applications are mainly related to petrochemical equipment, salt production equipment, and thermal power generation equipment. With the development of marine resources, the applications of titanium/steel composite plates become more common in marine oil and gas exploitation, port construction, coastal power stations, seawater desalination, shipping, marine fisheries, and marine thermal energy conversion[1–5].

At present, the primary methods for producing titanium/steel composite plates include explosive welding, explosive-rolling, diffusion bonding, and hot rolling. Furthermore, laser engineering net shaping[6], discharge plasma sintering[7], jet deposition[8], and brazing composite[9–10] methods have also been used to fabricate titanium/steel composite plates, but these methods are currently restricted to laboratory studies. Currently, explosive welding, a specialized welding technique using large energy produced by explosive detonation to drive high-speed oblique collisions between metal plates, is still the most common method. The explosive welding method features a straightforward production process to bond dissimilar metals with significant physical and chemical property differences. Additionally, the welding duration is very short, allowing for effective control over the formation of intermetallic compounds, thus ensuring high bonding quality. Nevertheless, the mechanization level of the explosive welding process is relatively low, so noise and pollution are inevitable, thereby restricting the further development and application[11].

The charge amount is a critical process parameter in explosive welding. An increase in amount of explosives heightens the likelihood of hazards during manual mixing. Additionally, environmental problems, such as noise, shock

Received date: December 15, 2024
Foundation item: Jiangsu Provincial Natural Science Foundation of China (BK20211232); 2023 Major Science and Technology Projects of Nanjing City (202309011)
Corresponding author: Jiang Jialin, Master, Army Engineering University of PLA, Nanjing 210007, P. R. China, E-mail: luoxuchuan@aeu.edu.cn

waves, and dust, resulting from explosions also become more serious with the increase in charge amount. Reducing the charge amount is beneficial to problem settlement and production cost reduction. Shi et al[12] proposed a dual vertical explosive welding and protective device by vertically arranging a set of metal pieces on either side of a sealed explosive charge. After the explosives were detonated using a detonator, the left and right sets of metals underwent explosive welding, which saved at least one-third of the explosive charge while maintaining excellent interface bonding quality. Yang et al[13] employed colloidal water for explosives and found that with colloidal water as a constraint, the critical thickness of the explosives could be reduced, and the dust and shock wave energy produced by the explosion could also be effectively absorbed by the colloidal water.

Selecting appropriate welding parameters is essential to enhance the quality of interface welding. Kahraman[14] and Manikandan[15] et al conducted explosive welding experiments on titanium/steel with different mass ratios. The results indicated that the hardness of the composite plate rose with an increase in mass ratio, and the peak hardness was at the interface. Wang[16] and Miao[17] et al performed explosive welding tests on titanium/steel under different gap conditions. The results demonstrated that the bonding quality of the interface was initially increased and then decreased with the increase in gap due to excessive collision energy. Zareie et al[18] conducted explosive welding experiments on nickel-based alloys and low-carbon steel with different mass ratios and gaps. The findings indicated that the shear strength was increased with the collision energy, and an optimal shear strength existed. Increasing the gap and mass ratio can promote the shear strength, but excessive collision energy will significantly lower the shear strength. Shi et al[19] introduced the lower limit principle for explosive welding, pointing out that a critical collision energy value exists for good interface bonding. By controlling the gap, the speed of flyer plate can be sufficiently accelerated to the maximum value with a small charge amount, achieving fine bonding with the base plate at the critical collision energy.

The extremely short duration of explosive welding leads to difficulties in observation of the entire experiment process, especially the formation process of the wavy interface. Therefore, numerical simulation techniques have been incorporated into the research of explosive welding. Due to the inherent characteristics of explosive welding, such as high temperature, high pressure, and high strain rates, it is challenging to measure dynamic parameters, such as the collision angle within the welding window. However, numerical simulation can effectively study various dynamic parameters. At present, the morphologies of explosively welded interfaces are mainly investigated through two-dimensional simulations. Ma[20], Bataev[21], and Wu[22] et al conducted numerical simulations to investigate the growth process of wave-like interface and analyzed the causes of wavy interfaces. Wu et al[22] further examined several groups of metal foils and plates, using smoothed particle hydrodynamics (SPH) and Euler numerical simulation methods to analyze the influence of collision parameters and wave impedance between the base and flyer plates on waveform characteristics. The evolution of three typical characteristic waveforms and the development of vortex structures were discussed. Nonetheless, the quantitative relationships between the parameters of experiment and numerical simulation are still obscure.

In this research, a weldability window for TA1/Q235 composite plate was established, the quantitative relationship between dynamic and static process parameters in TA1/Q235 explosive welding was proposed, and the lower limit of explosive charge amount required for welding was investigated. This study employed two-dimensional numerical simulations based on dynamic process parameters, such as collision speed and collision angle, and conducted explosive welding using static process parameters, including explosive thickness and gap. Explosive welding tests were conducted on TA1 flyer plates with thickness of 1, 2, and 4 mm and Q235 base plates with thickness of 8 mm, and the explosive thickness was 25 mm. This research provided reference for the further investigation of explosive welding of TA1/Q235 composite plates.

2 Theoretical Calculation

2.1 TA1/Q235 weldability window

The weldability window is a tool used to determine the feasible range of dynamic process parameters in explosive welding and to predict welding quality. A theory of the weldability window has been proposed based on the collision angle (β) and welding speed (V_c) for explosive welding. The weldability window consists of four components: the upper welding limit, the lower welding limit, the flow limit, and the sound speed limit.

Carpenter et al[24] examined the energy transfer during the explosive welding process and defined the upper welding limit as the condition that the heat generated by the collision does not produce a continuous molten layer at the interface. Thus, the upper welding limit is expressed by Eq. (1), as follows:

$$\sin(\beta/2) = \frac{\left(T_m C_0\right)^{1/2}}{2NV_c^2}\left(\frac{kC_pC_0}{\rho_f\delta_f}\right)^{1/4} \quad (1)$$

where T_m represents the melting point of the metal with the lowest melting point in the composite plate materials; k is the thermal conductivity; C_p is the specific heat capacity at constant pressure; C_0 is the bulk sound speed; ρ_f is the density of the flyer plate; δ_f is the thickness of the flyer plate; N is a constant of 0.11. All these parameters, except T_m, are taken from the flyer plate.

Deribas et al[25] found that the impact load generated by the collision of the flyer plate and base plate must exceed the dynamic strength of the material to ensure the generation of a metal jet, which effectively cleans the interface. This result defined the lower limit of welding speed, as expressed by Eq.(2), as follows:

$$V_c = \frac{k_1}{\beta}\sqrt{\frac{H_v}{\rho_f}} \quad (2)$$

where k_1 is a constant related to the cleanliness of the material surface with a typical value of 0.85, ranging from 0.6 (high cleanliness) to 1.2 (low cleanliness); H_v represents the Vickers hardness of the material; ρ_f is the density of the flyer plate.

Zakharenko et al[26] indicated that when the hardness difference of the to-be-welded metals is significant, H_v should be the hardness of the relatively soft material, and k_1 should be set as 1.14.

Wang et al[27] indicated that the flow limit corresponds to the minimum welding speed during explosive welding to ensure that the material reaches a flowing state in the jet region. Thus, the flow limit is as follows:

$$V_c = \sqrt{20R_{max}/\rho_{min}} \quad (3)$$

where R_{max} is the maximum tensile strength of the to-be-welded metals; ρ_{min} is the minimum density among the to-be-welded metals.

Li et al[28] argued that as V_c increases, the collision angle β decreases, leading to the supersonic collision of the base and flyer plates. In this case, the base and flyer plates are immediately bounced apart after collision, thus preventing the generation of a jet. For the theoretical sound speed limit, the speed of the shock wave in metals can be determined by a collision model. Since the sound speed limit for most materials is relatively high, it can be simply considered in engineering that V_c should be less than the material sound speed, as follows:

$$V_c = \min(C_{01}, C_{02}) \quad (4)$$

where C_{01} and C_{02} represent the wave sound speed of the base and flyer plate materials, respectively. It is worth noting that since the sound speed of most metallic materials is 4–5 km/s, situations with V_c exceeding the sound speed limit are rare in considered.

During explosive welding, the kinetic energy of the flyer plate is primarily derived from the energy provided by the detonation products of the explosive under the influence of detonation. Consequently, the ratio of explosive mass per unit area to the flyer plate mass per unit area is a key factor influencing the motion posture of the flyer plate. The ratio of the explosive mass per unit area to the mass of flyer plate per unit area is defined as the mass ratio (R), which is expressed by Eq.(6), as follows:

$$R = \frac{\rho_e \delta_e}{\rho_f \delta_f} \quad (6)$$

where ρ_e is the explosive density; δ_e is the explosive thickness; ρ_f is the density of flyer plate; δ_f is the thickness of flyer plate.

production practice. In the case of welding the low-sound-speed alloys (sound speed of around 2 km/s), the influence of the sound speed limit must be considered.

The material parameters of the base and flyer plates are provided in Table 1. By substituting these parameters into Eq.(1 – 4), the weldability window of explosive welding of TA1/Q235 composite plate with flyer plate thicknesses of 1, 2, and 4 mm can be established, as depicted in Fig.1.

2.2 Process parameters of TA1/Q235 explosive welding

The parameters of the explosive welding process can be divided into dynamic process parameters and static process parameters. The dynamic process parameters mainly include the collision velocity of the base and flyer plates (V_p), the welding velocity (V_c), and the collision angle (β). The static process parameters primarily consist of the explosive thickness (δ_e), the detonation velocity of the explosive (V_d), and the gap between the base and flyer plates (s). In the parallel explosive welding method, as shown in Fig. 2, the welding velocity (V_c) is equal to the detonation velocity (V_d). Based on the geometric and mechanical relationships of the motion posture of the base and flyer plates, a mathematical relationship between the collision velocity (V_p) and the detonation velocity (V_d) can be derived, as follows:

$$V_p = 2V_d \sin(\beta/2) \quad (5)$$

For explosive welding process, once the base plate material is selected, it is also necessary to determine the static process parameters, such as the explosive thickness (δ_e). The range of dynamic process parameters can be obtained from the previously established weldability window of TA1/Q235 composite plate. Furthermore, it is essential to further ascertain the quantitative relationship between the dynamic and static process parameters to fabricate composite plates. When the dynamic parameters are transformed into static parameters, such as explosive thickness and gap, the motion of the flyer plate driven by the explosive detonation must be

For the motion of the flyer plate driven by explosive detonation, various one-dimensional and two-dimensional detonation-driven models have been proposed. One-dimensional Gurney equation uses the simplest one-dimensional expansional mechanics model with the initiation form of constant volume detonation, as expressed by Eq.(7–8)[29], as follows:

$$E = \frac{1}{\gamma^2 - 1}\left(\frac{\gamma}{\gamma + 1}\right)^{\gamma} V_d^2 \quad (7)$$

$$V_p = \left(\frac{6ER}{5 + R + 4/R}\right)^{1/2} \quad (8)$$

where E represents the Gurney coefficient; γ is effective multi-directional exponent of the explosive.

Therefore, by combining Eq.(6–8), a quantitative relationship

Table 1 Material parameters of base plate and flyer plate

Material	T_m/K	C_0/m·s^{-1}	C_p/J·kg^{-1}·K^{-1}	k/W·m^{-1}·K^{-1}	H_v/GPa	Density, ρ/kg·m^{-3}	Tensile strength, R_m/GPa
TA1	1944	5020	550	15	1.6	4500	0.441
Q235	1766	4569	452	38	1.7	7850	0.405

of the relevant parameters of the explosive, flyer plate, and collision velocity can be established, as shown in Eq. (9). By combining Eq. (5–9), a relationship of explosive, flyer plate, and collision angle can be derived, as shown in Eq.(10).

$$V_p = \left(\frac{\gamma}{\gamma+1}\right)^{\gamma/2} V_d \left[\frac{6\rho_e^2\delta_e^2}{(\gamma^2-1)(5\rho_e\delta_e\rho_f\delta_f+\rho_e^2\delta_e^2+4\rho_f^2\delta_f^2)}\right]^{1/2} \tag{9}$$

$$\beta = 2\arcsin\left\{\frac{1}{2}\left(\frac{\gamma}{\gamma+1}\right)^{1/2}\left[\frac{6\rho_s^2\delta_s^2}{(\gamma^2-1)(5\rho_s\delta_s\rho_f\delta_f+\rho_s^2\delta_s^2+4\rho_f^2\delta_f^2)}\right]^{1/2}\right\} \tag{10}$$

When the one-dimensional detonation-driven model is used, the initiation form has a significant impact on the acceleration process of the flyer plate, but a lesser effect on the final velocity of the flyer plate. Therefore, the one-dimensional detonation-driven model has good accuracy to address the terminal velocity issue of the flyer plate in explosive welding. However, when the mass ratio (R) exceeds 3 and the effective multi-directional exponent of the explosive (γ) is less than 2, significant discrepancies can arise in the calculation results of the one-dimensional detonation-driven model. Li et al[28] addressed the case where the effective multi-directional exponent of the explosive (γ) is less than 2. They established the Richter model and applied a characteristic line method from compressible fluid dynamics to fit and organize the characteristic line differential calculation results into empirical formulas to derive the corresponding velocities of the flyer plate during the acceleration phase, as follows:

$$\frac{s}{\delta_e} = \frac{(\gamma+1)\beta_m}{R}\left[\frac{\beta^3}{18}+\frac{\beta_m\beta^2}{12}+(\beta_m^2-1)\beta + (\frac{\beta_m^3}{6}-\beta_m)\ln\left(1-\frac{\beta}{\beta_m}\right)\right] \tag{11}$$

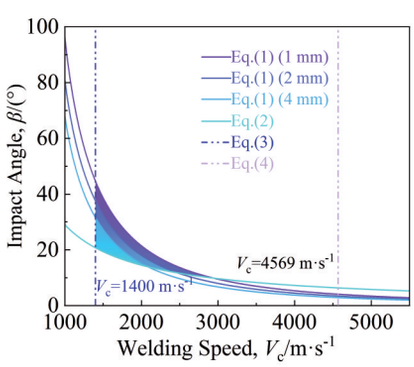

Fig.1 Weldability window of explosive welding of TA1/Q235 composite plate

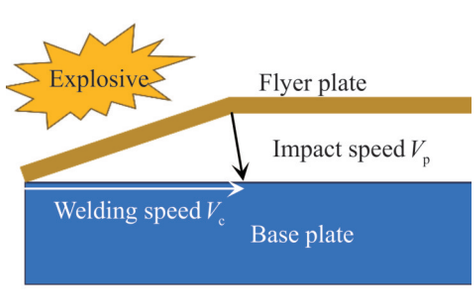

Fig.2 Schematic diagram of parallel explosive welding

$$\frac{1}{\beta_m} = 0.5634\gamma + 0.4509 + (1.0785\gamma - 0.2598)/R \tag{12}$$

where β_m is the maximum collision angle.

The detonation velocity of the explosive is also an important factor affecting the quality of interfacial bonding. Based on the weldability window for explosive welding, the detonation velocity of the explosive should be lower than the bulk sound velocity of the base and flyer plate materials. Moreover, the slower the detonation velocity, the larger the theoretical thickness of the explosive. Larger theoretical explosive thickness improves the adjustability of the explosive detonation capability. Therefore, within the weldability window, explosives of slow detonation velocity, such as 53# (a powdery emulsified explosive mixed uniformly with 53% quartz sand and a small amount of sawdust), were chosen for experiments. This explosive has a detonation velocity of approximately 1800 m/s, a density of about 1.0 g/cm^3, and an effective multi-directional exponent of the explosive of approximately 1.5.

The "yield-tensile" primary criterion[30] points out that the condition for successful explosive welding of composite plates is that the maximum bending moment caused by the detonation load on the flyer plate must be greater than the bending moment of the flyer material at the dynamic yield limit and less than the bending moment at the dynamic tensile strength. This condition leads to a novel expression for the lower limit of explosive thickness, as follows:

$$\delta_{e_{min}} \geqslant l\cot\frac{l}{\omega}\arccos\sqrt[m]{45R_{eL}\delta_f^2(1+\gamma_H)/\rho_e V_d^2 l^2 - 2} \tag{13}$$

$$m = 2\gamma/(\gamma-1) \tag{14}$$

$$\omega = \sqrt{(\gamma-1)/(\gamma+1)} \tag{15}$$

where R_{eL} is the yield limit of the flyer material; δ_f is the thickness of the flyer plate; ρ_e is the density of the explosive; V_d is the detonation velocity of the explosive; l is the effective interaction distance; γ is the effective multi-directional exponent of the explosive; γ_H is the effective multi-directional exponent of the detonation wave front.

The "yield-tensile" primary criterion can effectively guide the practical production of explosive welding. However, after production following this primary criterion, a slight interfacial melting can be observed at the bonding interface by optical microscope (OM), as shown in Fig.3. The process parameters are listed in Table 2. The presence of interfacial melting indicates that explosive thickness is excessive, therefore leading to a high collision energy. The fundamental condition for explosive welding is an inclined collision between the base and flyer plates, so the flyer plate undergoes bending deformation. However, reaching the dynamic yield limit is not

a sufficient and necessary condition for bending deformation. Therefore, it is assumed that the maximum bending moment caused by the detonation load on the flyer plate does not need to exceed the bending moment of the flyer material at the dynamic yield limit. Accordingly, the explosive thickness of 25 mm, which is calculated based on the "yield-tensile" criterion for TA1 flyer plate with thickness of 1 mm, may be excessively large, and this explosive thickness may provide fine bonding between the flyer plate with thickness greater than 1 mm and the base plate. To verify this assumption, the critical explosive thickness of 25 mm was used to conduct explosive welding experiments on TA1 flyer plates with thicknesses of 1, 2, and 4 mm and Q235 base plates with thickness of 8 mm.

After determining the parameters of the base and flyer plates as well as the explosive, the gap between the flyer and base plate should also be determined. Blazynski et al[31] noted that when the gap is sufficiently large, the motion of the flyer plate can be divided into three phases: accelerated, constant, and decelerated. The accelerated phase can be further divided into rapid and slow acceleration stages. Because an excessively large gap increases the difficulty of gas venting, the upper limit of the gap should fall within the range of the slow acceleration stage of flyer plate. This settlement allows the flyer plate to accelerate adequately while avoiding excessive venting difficulties. For an explosive composed of 80/20 plastic explosive, the distances for accelerating the velocity of titanium plates with thickness of 1, 2, and 4 mm to their maximum value are 5.2, 7.1, and 9.8 mm, respectively. Considering the differences in explosive type and explosive thickness and the fact that the upper limit gap needs to be within the range of slow acceleration stage of the flyer plate, the gap should be slightly smaller than these values. Furthermore, since the explosive welding of the flyer plate with thickness of 1 mm belongs to the thin plate explosive welding, it is important to avoid excessive acceleration, which may lead to overheating at the interface. Therefore, for the TA1 flyer plates with thicknesses of 1, 2, and 4 mm, the gaps were set as 3, 6, and 8 mm, respectively. Since the flyer plate with thickness of 1 mm does not have sufficient speed, the calculations will be conducted using Eq.(11–12). For the flyer plates with thickness of 2 and 4 mm, it can be assumed that their speed is enough, so the calculations will be conducted using Eq.(10).

When the explosive thickness (δ_e) is 25 mm, the thickness of base plate (δ_j) is 8 mm, and the thickness of flyer plate (δ_f) is 1, 2, and 4 mm, the resulting collision speed (V_p) and collision angle (β) are listed in Table 2, which all fall within the weldability window.

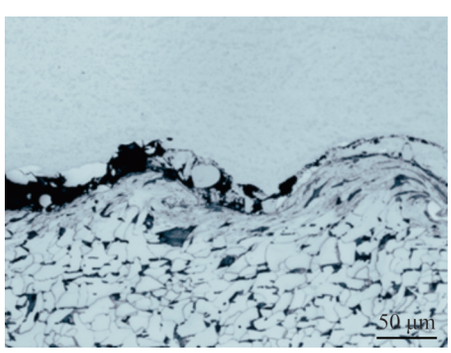

Fig.3 OM image of interface melting

Table 2 Collision velocity and collision angle under different conditions

δ_e/mm	δ_j/mm	δ_f/mm	V_p/m·s^{-1}	β/(°)
25	8	1	760.50	24.39
25	8	2	667.47	21.37
25	8	4	579.60	18.53

Note: δ_j is the thickness of base plate

3 Numerical Simulation and Tests

3.1 Numerical simulation

3.1.1 β-V_p high-speed oblique collision model

During the explosive welding process, the flyer plate undergoes bending deformation under the driving force of explosive detonation, colliding with the base plate at a certain speed (collision speed V_p) and a certain angle (collision angle β), and achieving a firm metallurgical bond under high temperature and high pressure. The parallel explosive welding can be simplified to a high-speed inclined collision model, as shown in Fig.4.

3.1.2 SPH algorithm

Two-dimensional numerical simulation of the TA1/Q235 explosive welding process is usually conducted using AUTODYN software. The traditional Lagrangian algorithm struggles with grid distortion during large deformation problems, while SPH algorithm does not rely on grid division and is suitable for large deformation issues. Therefore, SPH algorithm was used for numerical simulation of the explosive welding process. The dimensions of base plates were 20 mm× 8 mm, and the dimensions of flyer plates were 20 mm×1 mm, 20 mm×2 mm, and 20 mm×4 mm with total particles (particle size was 0.02 mm) of 450 000, 500 000, and 600 000, respectively.

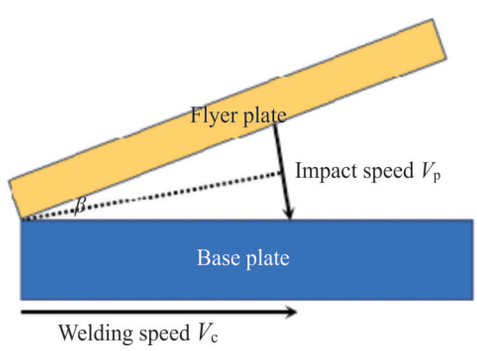

Fig.4 High-speed oblique collision model

3.1.3 Material constitutive model and state equation

Explosive welding represents a typical behavior of materials under large deformation and high strain rates. The materials of the base and flyer plates undergo severe collision under explosive detonation pressure and thermal effects, resulting in high temperatures, high pressures, and significant deformation.

The Johnson-Cook material constitutive model is suitable to solve the high-speed collisions and strong shock loads caused by explosive detonation, as follows:

$$T^* = (T-T_r)/(T_m-T_r) \tag{16}$$

$$\sigma = (1-T^{*m})(A + B\varepsilon_p^n) + (1 + C\ln\varepsilon_p^*) \tag{17}$$

$$\varepsilon_p^* = \varepsilon_p/\varepsilon_p^0 \tag{18}$$

where T_r is the environment temperature; T_m is the melting point of the material; T^* is a dimensionless temperature; A, B, C, m, and n are material-specific coefficients; ε_p is effective plastic strain; ε_p^0 is the reference strain rate; ε_p^* is effective plastic strain rate.

The Johnson-Cook material constitutive model requires an equation of state for the solid elements. Then, the Mie-Gruneisen equation of state was chosen, which effectively simulates the relationship between volume and internal energy of the material under pressure. The specific parameters for the constitutive models and equations of state for the base and flyer plate materials are detailed in Table 3. The Mie-Gruneisen equation of state can be represented as follows:

$$p = \frac{\rho_0 C_0^{\,2}\left[1 + \left(1-\frac{\gamma_0}{2}\right)\mu - \frac{a}{2}\mu^2\right]}{\left[1-(S_1-1)\mu - S_2\frac{\mu^2}{\mu+1} - S_3\frac{\mu^3}{(\mu+1)^2}\right]^2} + (\gamma_0 + a\mu)E \tag{19}$$

where S_1, S_2, and S_3 are fitting coefficients; γ_0 is the Gruneisen coefficient; a is the volume correction factor; C_0 is the bulk sound velocity of the material; ρ and ρ_0 are the current and initial densities of the material, respectively; $\mu=\rho/\rho_0-1$.

3.2 Tests

Industrial pure titanium TA1 was used as the flyer plate, and carbon structural steel Q235 was used as the base plate. The dimensions of base plates were 300 mm×150 mm×8 mm, and the dimensions of flyer plates were 300 mm×150 mm×1, 2, or 4 mm. The explosives were type 53# explosive with a detonation velocity of approximately 1800 m/s, density of about 1.0 g/cm^3, and effective multi-directional exponent of approximately 1.5. All tests employed a central detonation method on the longer edge with gap of 3, 6, and 8 mm and a consistent explosive thickness of 25 mm. Before the tests, the contact surfaces of the base and flyer plates were ground with a grinding wheel and then coated with a butter layer.

As shown in Fig. 5, the composite plates are free of holes and cracks, and no surface ablation can be observed, showing excellent bonding.

In order to conduct mechanical performance tests and microstructural observation of the composite plate interface while minimizing the use of composite plate material, the samples was cut according to the wire cutting scheme for each test, as shown in Fig.6.

Samples 1# – 3# were ground and polished with the titanium side etched by Kroll's reagent and the steel side etched by 4vol% nitric acid ethanol reagent. Samples 1# – 3# underwent analysis of OM, scanning electron microscope, energy dispersive spectrometer (EDS), electron backscattered diffractometer (EBSD), and microhardness tester. The impact toughness tests for samples 4# – 5# were conducted at room temperature using a fully automated computer-controlled metal pendulum impact testing machine (PIT-452D/LH-L-12/450J). Load-shear tests for samples 6# – 7# were performed using an electronic universal testing machine (WDW-300E/LH-L-03). Sample 8# was subjected to an internal bending test using a hydraulic servo universal testing machine (WAW-1000D/LH-L-02), while sample 9# was tested for external bending. The impact toughness tests were conducted in accordance with GB/T 229-2007, the load-shear tests followed GB/T 6396-2008, and the bending tests were conducted according to GB/T 232-2010.

Table 3 Parameters of material constitutive model and equation of state of base plate and flyer plate

Material	ρ/kg·m^{-3}	T_r/K	T_m/K	A/GPa	B/GPa	n	C	m	C_0/km·s^{-1}	S_1	γ_0	a
TA1	4500	300	1944	0.42	0.38	0.32	0.22	0.70	5.02	1.028	1.40	0.00
Q235	7850	300	1766	0.792	0.51	0.26	0.014	1.03	4.569	1.49	2.17	0.46

Fig.5 Composite plates with different flyer plate thicknesses after explosion and mechanical tests: (a) 1 mm; (b) 2 mm; (c) 4 mm

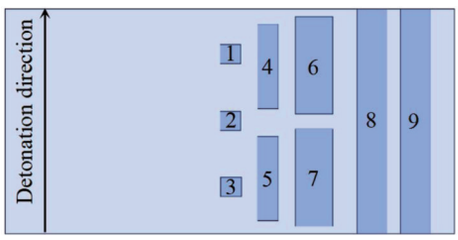

Fig.6 Wire cutting scheme of composite plate after explosion

4 Analysis of Test and Simulation Results

4.1 Analysis of mechanical test results

4.1.1 Impact toughness analysis

The impact absorption work (impact energy) of the samples from composite plates with different flyer plate thicknesses is shown in Table 4. Because the flyer plate thickness is 9 mm, it is impossible to prepare the standard sample of 55 mm×10 mm×0 mm. Instead, a small sample of 55 mm×10 mm×7.5 mm was prepared according to GB/T 229-2007, and its corrected impact absorption work is 157 J. The average impact absorption work of composite plate with flyer plate thickness of 4 mm is only 81 J, because the original thickness of the flyer plate is retained during the preparation of the impact sample. The base plate of 2 mm is removed, resulting in a larger proportion of titanium, which has a lower impact absorption work. This phenomenon leads to fact that the measured impact absorption work of the sample from composite plate with flyer plate thickness of 4 mm is lower than that of 1 and 2 mm. According to GB/T 700-2006, the impact absorption work of Q235 (V-notched) should not be less than 27 J. Therefore, it can be seen that the impact toughness of composite plates with different flyer plate thicknesses far exceeds that of the base material standard.

Table 4 Impact energy and shear strength of composite plates with different flyer plate thicknesses

Thickness/mm	Impact energy/J			Shear strength/MPa		
	Sample 4#	Sample 5#	Mean value	Sample 6#	Sample 7#	Mean value
1	111	125	118	354	376	365
2	157	166	162	348	321	335
4	90	71	81	375	423	399

4.1.2 Shear property analysis

The magnitude of the shear strength of the composite plate typically reflects the strength of the interface bonding, and it is an important indicator to evaluate the quality of the composite plate[32]. As shown in Table 4 and Fig. 7a–7c, the average shear strength of the samples from composite plates with flyer plate thickness of 1, 2, and 4 mm is 365, 335, and 399 MPa, respectively. According to GB/T 8547-2019, the shear strength of Class 0 titanium-steel explosive composite plates should not be less than 196 MPa; while for Class 1 and Class 2 explosively welded titanium/steel composite plates, it should not be less than 140 MPa. Therefore, it can be concluded that composite plates prepared in this research are fully capable to be considered as high-strength Class 0

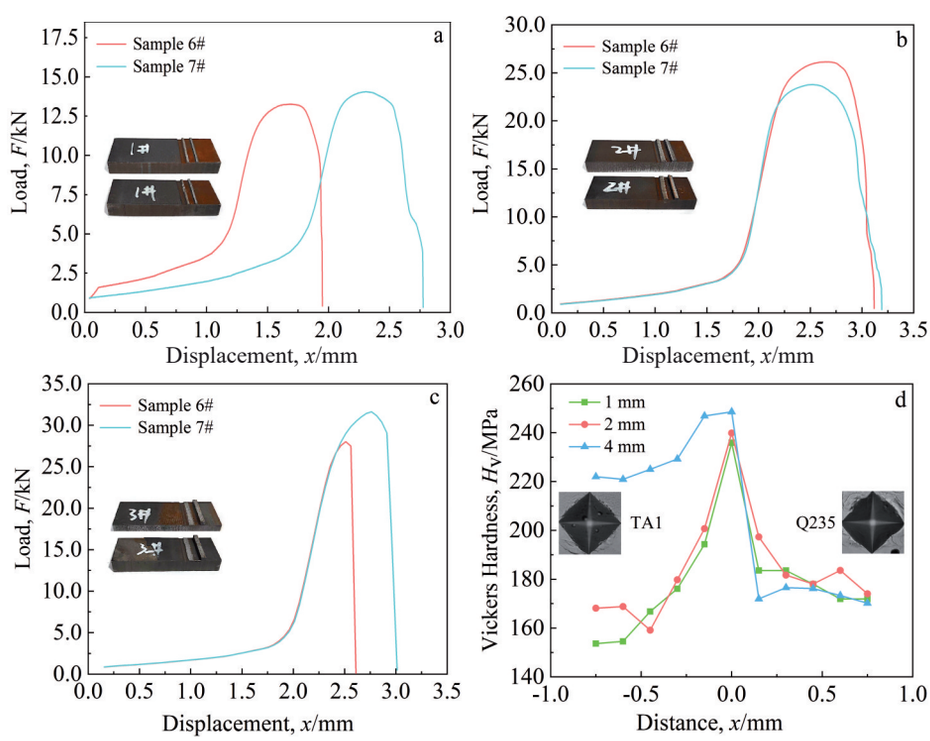

Fig.7 Shear strength of composite plates with flyer plate thickness of 1 mm (a), 2 mm (b), and 4 mm (c); Vickers hardness of composite plates with different flyer plate thicknesses (d)

composite plates.

4.1.3 Bending property analysis

Both inner bending at 180° (TA1 on the inside) and outer bending at 180° (TA1 on the outside) tests were conducted to observe whether the delamination or cracking occurs at the bonding interface. The dimensions of the bending samples for composite plates with different flyer plate thicknesses are 150 mm×20 mm×9, 10, or 12 mm. The results are shown in Fig.7a – 7c. The inner bending samples from composite plates with flyer plate thickness of 1, 2, and 4 mm and the outer bending samples from composite plates with flyer plate thickness of 2 and 4 mm maintain intact bonding interfaces and material matrices, whereas the titanium side surface of the outer bending sample of composite plate with flyer plate thickness of 1 mm experiences cracking, although the bonding interface is not delaminated. This result indicates that the bonding strength of composite plates can satisfy the requirements. The cracking on the titanium side of the outer bending sample of composite plate with flyer plate thickness of 1 mm may be attributed to its thinner titanium matrix coupled with severe plastic deformation under the direct action of the explosion load, leading to work hardening and subsequently reducing the plasticity and toughness.

4.1.4 Microhardness analysis

Microhardness infers the capacity of a material to resist plastic deformation caused by applied forces. The microhardness near the composite interface of the samples was tested using the Vickers indentation method with a load of 4.9 N, holding time of 10 s, and spacing of 0.15 mm between indentations. The experiment results are shown in Fig.7d. The composite plates with flyer plate thickness of 1, 2, and 4 mm exhibit the maximum microhardness at the interface as 235.88, 239.88, and 248.54 MPa, respectively. Furthermore, the further the distance from the bonding interface, the smaller the microhardness. In the end, the microhardness of the composite plate is basically equal to that of the original matrices. Notably, the microhardness on the steel side of composite plates tends to be stable at 170 MPa, whereas the microhardness on titanium side of composite plates with flyer plate thickness of 1, 2, and 4 mm tends to 150, 170, 220 MPa, respectively. The microhardness decrement of the titanium side of the composite plate with flyer plate thickness of 4 mm is the smallest. This is likely due to different degrees of plastic deformation occurring during explosive welding, resulting in varying levels of work hardening. With the decrease in distance to the interface, the plastic deformation degree increases, resulting in more significant work hardening and a higher microhardness value.

4.2 Interface microstructure

4.2.1 Waveform dimension analysis

The interface microstructure of explosive composite shows a wavy bonding feature between TA1 and Q235 sides (Fig.8). The interface of the composite plate with flyer plate thickness of 4 mm is the furthest from the detonation point and exhibits the most stable detonation speed among the three composite plates. The average wavelengths at this position of composite plates with flyer plate thickness of 1, 2, and 4 mm is 591, 783, and 456 μm with the average wave height of 140, 152, and 73 μm, respectively. It is reported that longer wavelengths in the wavy interface of explosively welded composite plates lead to larger areas of vortex structures and more metallurgical defects in the cast structure, adversely affecting the bonding strength at the interface. According to Fig.8, as the detonation distance increases, the wave dimensions of the interfaces in all

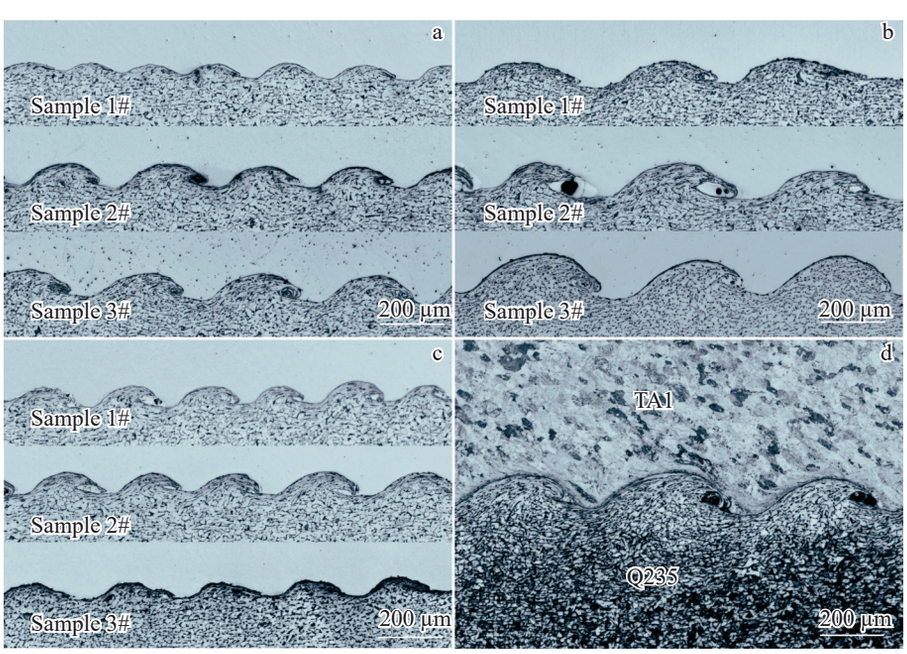

Fig.8 OM images of bonding interfaces of composite plates with flyer plate thickness of 1 mm (a), 2 mm (b), and 4 mm (c); magnified image of bonding interface of sample 3# of composite plate with flyer plate thickness of 2 mm after corrosion on both titanium side and steel side (d)

composite plates also increase. Furthermore, the composite plate with flyer plate thickness of 2 mm exhibits the largest wave dimension, followed by composite plate with flyer plate thickness of 1 mm, and the composite plate with flyer plate thickness of 4 mm has the smallest wave dimension. This result correlates with the shear strength, where the composite plate with flyer plate thickness of 4 mm has the highest shear strength, followed by composite plate with flyer plate thickness of 1 mm, and the composite plate with flyer plate thickness of 2 mm has the lowest shear strength.

4.2.2 Analysis of element mixing phenomenon

As shown in Fig. 8d, the steel side structure consists of pearlite and ferrite, while the titanium side contains *α*-titanium. The metallic grains on the steel side of the bonding interface are significantly elongated with vortex-like structures near the valley area. Vortex-like structures are typical morphology features of explosively welded composite interfaces. The substrate material experiences violent mechanical stirring under high temperature and high pressure in the vortex region, leading to defects of melted blocks, gas bubbles, and cracks after rapid cooling. Nevertheless, even these defects exist in the vortex region, the constraints from their boundaries still hinder their propagation under load, thus ensuring the high bonding strength of the interface. As shown in Fig. 9, the measurement points are evenly distributed within the vortex structure and raw material matrix, and the lines are indicated by the arrows. EDS analysis results are shown in Table 5 and Fig. 10. According to EDS point scanning results, element mixing can be observed in the vortex structures of composite plates. With the increase in flyer plate thickness, the extent of mixing becomes more pronounced. As shown in Fig. 10, the element mixing occurs in the vortex structures, and the composite plate with flyer plate thickness of 4 mm shows the most pronounced mixing phenomenon, which is indicated by the X-shaped crossover of the element distribution curves.

4.2.3 EBSD analysis results

The transformation of grain structure is influenced by a variety of thermodynamic factors, including temperature, pressure, and deformation. Because the materials near the interface of the substrate and the composite plate are under extreme conditions of high temperature, high pressure, and high strain rate during explosion welding, it is expected that a complex spatial distribution of grain structures exists in that region. EBSD analysis was conducted at the peak region of sample 3# from composite plate with flyer plate thickness of 1 mm, and the results are presented in Fig. 11. Fig. 11a depicts the inverse pole figure at the peak region, indicating that the grain distribution on the Q235 side varies markedly with distance to the interface. The grains close to the interface are primarily fine equiaxed grains. With the increase in distance, a deformation zone of 50 – 100 μm in width emerges, mainly consisting of elongated deformed grains interspersed with a

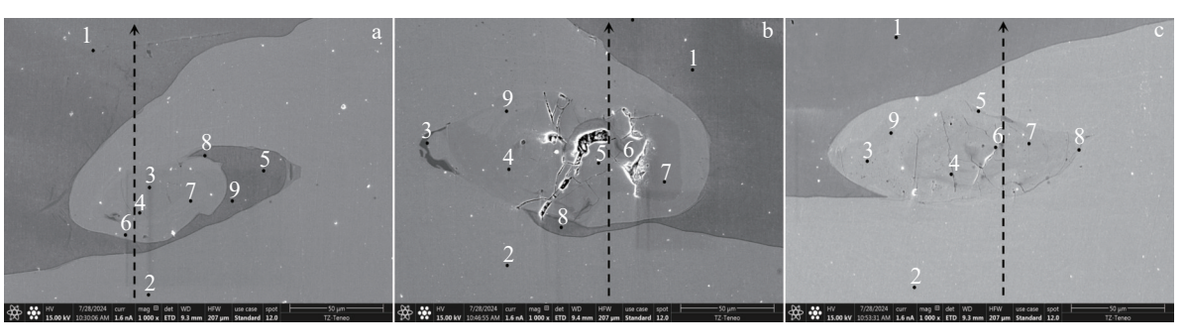

Fig.9 Positions of points and lines for EDS analyses at vortex region of composite plates with flyer plate thickness of 1 mm (a), 2 mm (b), and 4 mm (c)

Table 5 EDS results of points marked in Fig.9 (at%)

Point	Composite plate with flyer plate thickness of 1 mm		Composite plate with flyer plate thickness of 2 mm		Composite plate with flyer plate thickness of 4 mm	
	Ti	Fe	Ti	Fe	Ti	Fe
1	97.67	2.33	99.83	0.17	99.82	0.18
2	0.08	99.02	0.08	99.92	0.00	100.00
3	1.19	98.81	96.34	3.57	30.03	69.97
4	23.86	76.14	30.96	69.04	41.74	58.26
5	99.01	0.99	2.10	97.9	23.16	76.84
6	21.39	78.01	34.10	65.9	46.59	53.41
7	15.58	84.42	35.65	64.35	28.38	71.62
8	98.68	1.32	98.68	1.32	38.63	61.37
9	98.43	1.57	25.93	74.07	0.66	99.34

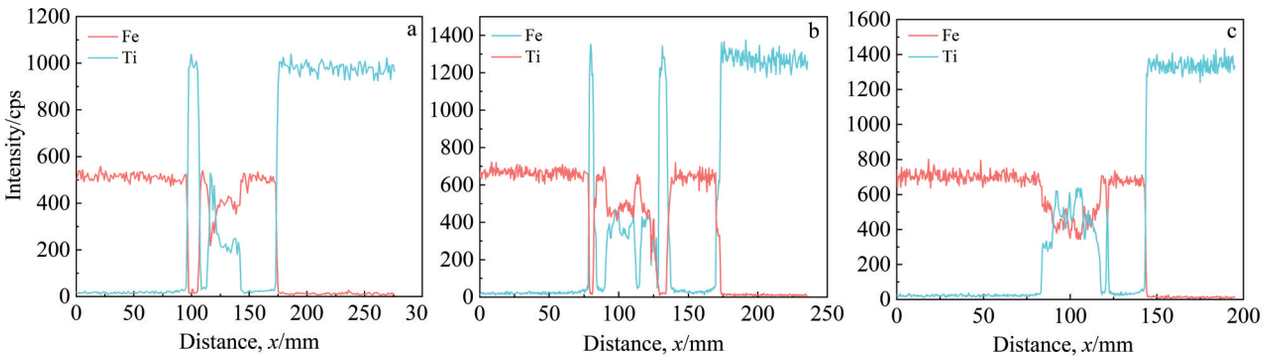

Fig.10 EDS line scanning results of vortex region of composite plates with flyer plate thickness of 1 mm (a), 2 mm (b), and 4 mm (c)

minor quantity of fine grains. Larger grains, exhibiting no noticeable deformation, are found far from the interface with diameters of approximately 20 μm. According to the grain size distribution diagram on the Q235 side (Fig.11e), it can be seen that the majority of grains on the steel side have diameters of less than 5.00 μm with the maximum grain diameter of 31.00 μm. The average grain size weighted by number is 3.91 μm, while that weighted by area is 13.98 μm. This phenomenon may be attributed to dynamic recrystallization occurring in the material adjacent to the interface under conditions of high temperature and high pressure coupled with rapid cooling, which restricts the complete growth of recrystallized grains, leading to the small sizes. With the increase in distance, the depth of the high-temperature and high-pressure region at the interface is restricted, suggesting that the dynamic recrystallization does not occur and resulting in significant plastic deformation under external forces to elongate the grains. As the distance from the heat-affected zone of the explosion welding continues to increase, the grain structure resembles that of the Q235 base material.

On the TA1 side, the majority of grains are small in size. The grain size distribution diagram of the TA1 side (Fig.11f) shows that the number-weighted average grain size is 3.24 μm, the area-weighted average grain size is 6.99 μm, and the

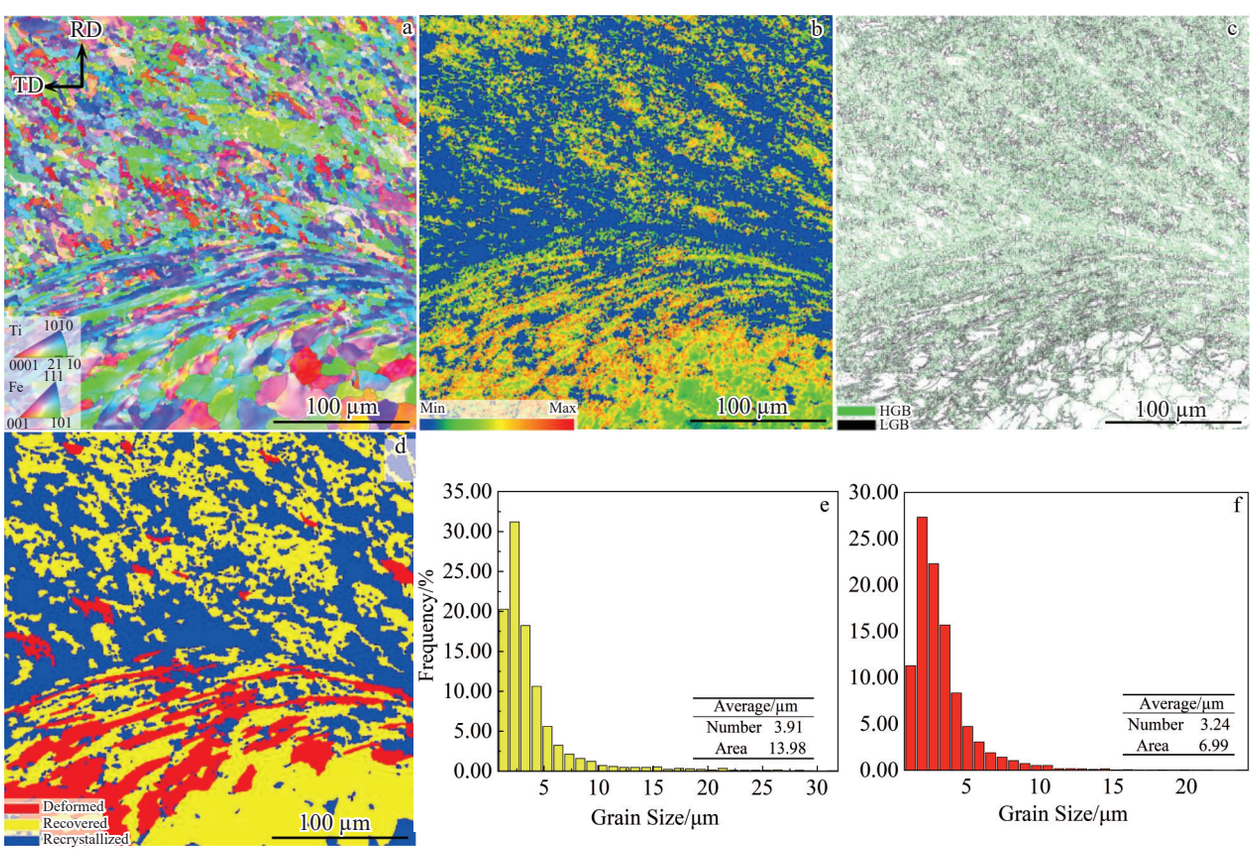

Fig.11 EBSD analysis results of peak region of sample 3# from composite plate with flyer plate thickness of 1 mm: (a) inverse pole figure; (b) kernel average orientation diagram; (c) grain boundary diagram; (d) grain orientation distribution diagram; (e) grain size distribution diagram at Q235 side; (f) grain size distribution diagram at TA1 side

maximum grain size is 23.00 mm. These small grains are primarily distributed near the interface and in several elongated regions (adiabatic shear bands) which are slightly farther from the interface. A small portion of these small grains are at the boundaries and interiors of larger grains. This phenomenon may result from the dynamic recrystallization in the regions near the interface and within the adiabatic shear bands, leading to grain size refinement. Additionally, severe plastic deformation causes grain refinement on the TA1 side, resulting in grain fragmentation.

Fig. 11b – 11d confirm the abovementioned hypothesis regarding the causes of grain distribution. Fig. 11b presents the kernel average orientation map of the measured region, which clearly illustrates the internal strain distribution in that area. During the recrystallization process, the emergence of new grains generally leads to the release of internal strains. Consequently, materials within the recrystallization zones often display lower strain levels. It can be seen that the areas near the bonding interface and the adiabatic shear bands demonstrate lower strain levels, confirming the occurrence of dynamic recrystallization in those regions. Conversely, the deformation zone on the Q235 side and other regions on the TA1 side, excluding the adiabatic shear bands, demonstrate elevated strain levels, suggesting that these areas experience intense plastic deformation. The grain boundary map (Fig.11c) reveals that most grain boundaries near the bonding interface and within the adiabatic shear band are high-angle grain boundaries (HGBs), while those in the deformation zone of the Q235 side and surrounding the adiabatic shear bands are predominantly low-angle grain boundaries (LGBs). The extensive generation of LGBs is attributed to the movement and rearrangement of dislocations, which result from strong plastic deformation[33]. During dynamic recovery and recrystallization, grain boundary migration is driven by strain and thermal energy, resulting in the conversion of LGBs to HGBs. The grain orientation distribution map (Fig. 11d) offers a more direct insight into the distribution of the deformed, recovered, and recrystallized grains. Most grains undergo the recrystallization process. In contrast, the regions on the TA1 side and the deformation zone on the Q235 side predominantly suffer severe plastic deformation.

Fig. 12 shows a strong fiber texture on the TA1 side, approaching the ideal {0001}//rolling direction (RD) texture. For {0001}, the density at both poles of RD axis is high; whereas at two poles and center point of the transverse direction (TD) axis, the density is comparatively lower, indicating that {0001} is nearly aligned with RD. Fig. 13 presents the pole figures on the Q235 side. In the case of {001}, the density peaks can be seen at angles of around 30° and 45° relative to RD axis, showing a strong Brass texture. Regarding {110}, the intensity peaks are noted at angles of approximately 45° and 60° relative to RD axis, demonstrating strong Brass and Copper textures. For {111}, the intensity peaks are observed at around 30° relative to RD axis and TD axis, indicating the strong Brass texture and the weak Copper texture. Shear deformation is an ideal process for texture formation. In the explosion welding process, high-speed oblique impacts generate intense shear stresses, causing some grains near the interface to uniformly deflect and resulting in preferred orientation[34].

4.3 Numerical simulation analysis results

4.3.1 Interface microstructure and distribution of pressure

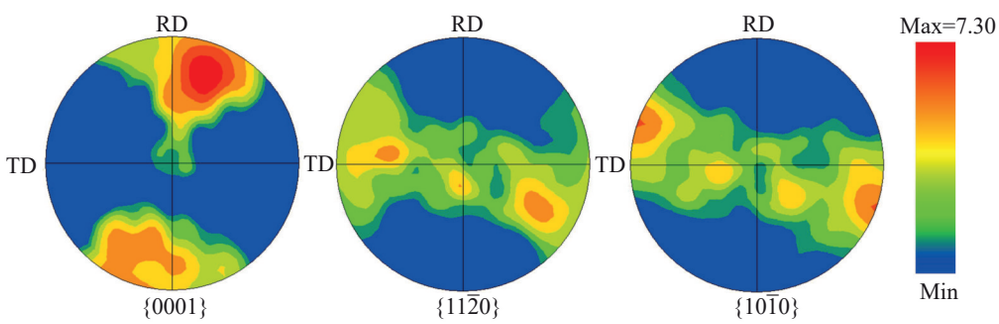

Fig.12 Pole figures on TA1 side of sample 3# from composite plate with flyer plate thickness of 1 mm

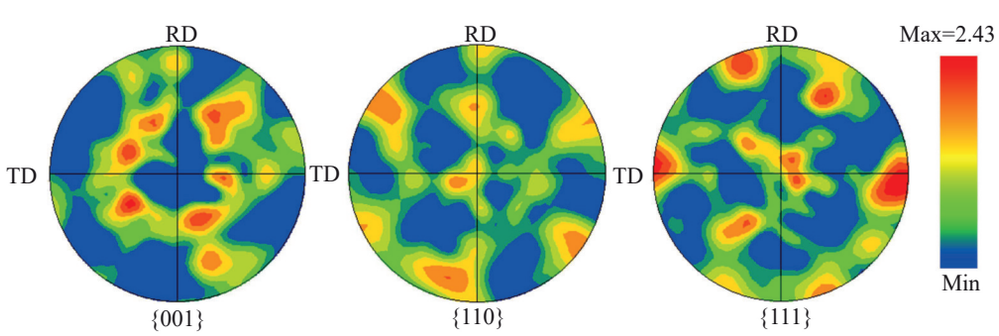

Fig.13 Pole figures on Q235 side of sample 3# from composite plate with flyer plate thickness of 1 mm

and temperature

Fig. 14 shows OM images and simulated morphologies of the bonding interfaces of composite plates with different flyer plate thicknesses, showing that the numerical simulation results align well with the experiment results. As shown in Fig. 15a, 22 gauge points are evenly distributed on the upper surface of the base plate and the lower surface of the flyer plate in three sets of simulation experiments, and the gauge point type was set to "Moving" to measure the pressure and temperature at each gauge point. The distribution of each gauge point after the explosive welding of composite plates with different flyer plate thicknesses is illustrated in Fig. 15b–15d. It is evident that in the simulation results, most gauge points placed on the Q235 substrate remain on the bonding interface, whereas only a few gauge points on the TA1 flyer plate are on the interface. The majority of gauge points are located in the jet at the right end, suggesting that the jet component in the TA1/Q235 composite plate primarily derives from the TA1 flyer plate. The pressure contour maps in Fig. 16 indicate a circular high-pressure region near the impact point. As shown in Fig. 16, a high-temperature zone adhering to the bonding interface can be observed, and the temperatures in the vortex and jet areas considerably exceed those in other regions. The vortex structure, caused by substantially higher temperature compared with that of surrounding areas, is prone to the formation of ingot structure defects, resulting in stress concentration at the interface and reducing the service strength of the composite plate. A notable degree of plastic deformation occurs at the interface, particularly in the vortex area, as shown in Fig. 16g–16i.

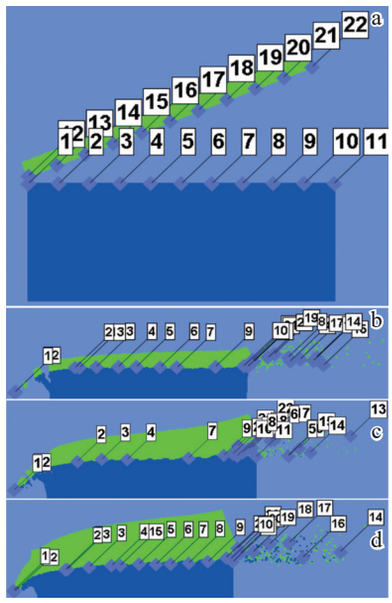

Fig.15 Gauge settings of composite plate with flyer plate thickness of 1 mm (a); final positions of gauges of composite plates with flyer plate thickness of 1 mm (b), 2 mm (c), and 4 mm (d)

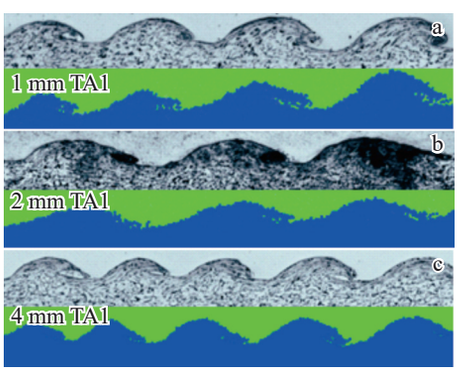

Fig.14 Comparison of interface morphologies and simulation results of composite plates with flyer plate thickness of 1 mm (a), 2 mm (b), and 4 mm (c)

Gauge points 2, 4, and 7 remain on the bonding interface during the simulation of explosive welding. Accordingly, these points are chosen as observation points to derive the historical data. Fig. 17a–17c present the temperature data at the observation points 2, 4, and 7 on the bonding interface of composite plates with different flyer plate thicknesses, revealing that the interface temperature quickly rises after the

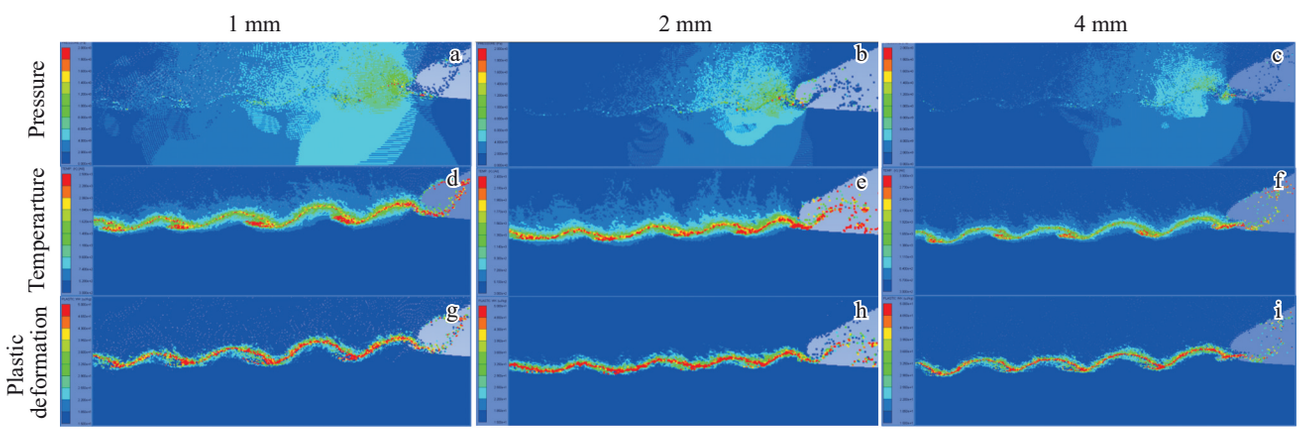

Fig.16 Numerical simulation results of composite plates with flyer plate thickness of 1 mm (a, d, g), 2 mm (b, e, h), and 4 mm (c, f, i): (a–c) pressure; (d–f) temperature; (g–i) plastic deformation

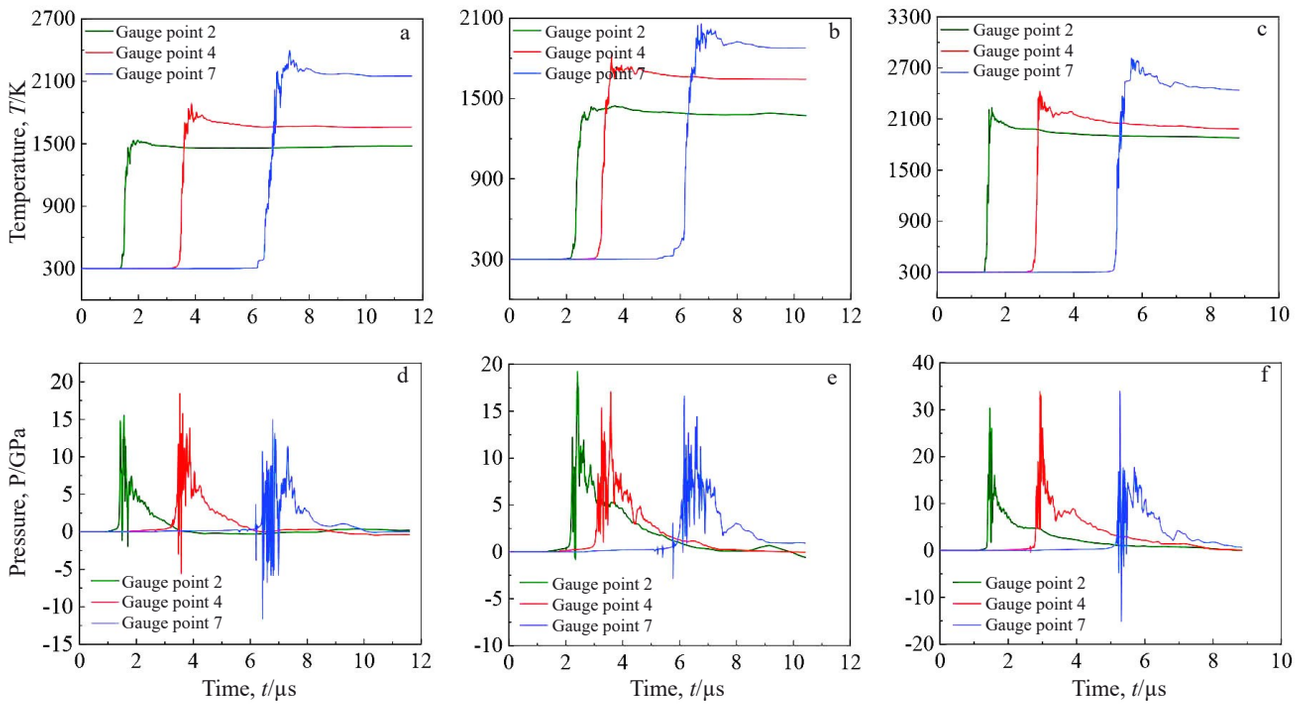

Fig.17 Temperature (a–c) and pressure (d–f) data of gauge points on composite plates with flyer plate thickness of 1 mm (a, d), 2 mm (b, e), and 4 mm (c, f)

collision and stabilizes after fluctuation. The peak temperatures at the observation points on composite plates with flyer plate thicknesses of 1, 2, and 4 mm are 2395, 2058, and 2813 K, respectively, and all the temperatures are much higher than the melting points of base and flyer plates. Fig.17d–17f show the pressure data at the observation points on the bonding interface of composite plates with different flyer plate thicknesses, indicating a rapid increase in interface pressure during the collision, followed by a swift decrease after the collision point. The observation points subject to both positive and negative pressures (positive pressure infers the compression and negative pressure infers tension). The peak pressures at three observation points on composite plates with flyer plate thicknesses of 1, 2, and 4 mm are 18.5, 19.2, and 34.1 GPa, respectively. The pressures all substantially exceed the yield limits of the materials. Therefore, it is evident that high temperature and high pressure are present at the collision point, causing the fluid-like mechanical behavior in a specific area near the bonding interface.

4.3.2 Interfacial jet flow and wave formation mechanism

The jet is fundamental to achieve explosive welding. The jet conditions at the interface of the base and flyer plates of composite plate with flyer plate thickness of 4 mm at different moments are shown in Fig. 18. It can be observed that a significant jet phenomenon occurs at the interface during the explosive welding process, and the jet oscillates periodically up and down within a certain angular range. It is clear that the jet at the interface forms before the collision point, incorporating components from both the substrate and flyer materials. Additionally, the jet near the flyer plate primarily consists of the material of the flyer plate, whereas the jet near the base plate mainly consists of the material of the base plate. The velocity of the interface jet can reach over 4500 m/s, and this high-speed interface jet effectively decreases the bonding interface, removing contaminants, metal oxides, and other impurities, and thus improving the quality of the interface bonding. Furthermore, the metallic jet remaining in the bonding interface is also an essential part of the formation of the interface waveform, where partial jet is captured by the substrate flow, resulting in a vortex morphology. Meanwhile, the high-pressure gas carried by the jet is captured by the substrate flow, leading to pore defects in the vortex structure.

To explore the formation mechanism of the explosively welded interface waveform structure, various mechanisms, including the penetration mechanism, fluid instability mechanism, Kármán vortex street mechanism, and stress wave mechanism have been proposed. Among these mechanisms, the penetration mechanism assumes that the material behaves like a non-viscous, incompressible fluid. When the metal flyer plate collides at an angle with the base plate, the flyer flow divides into two streams: one stream re-enters the flyer flow, while the other forms the jet. The jet penetrates the base plate, creating a pit. The material accumulates in front of the pit to form a bump, which continues to grow until the flyer flow captures the jet. After that, the collision point moves to the top of the bump and then descends, forming a new bump. This process is repeated several times, creating a continuous waveform. This mechanism aligns well with experiment observations. However, it cannot describe the fact that the substrate also

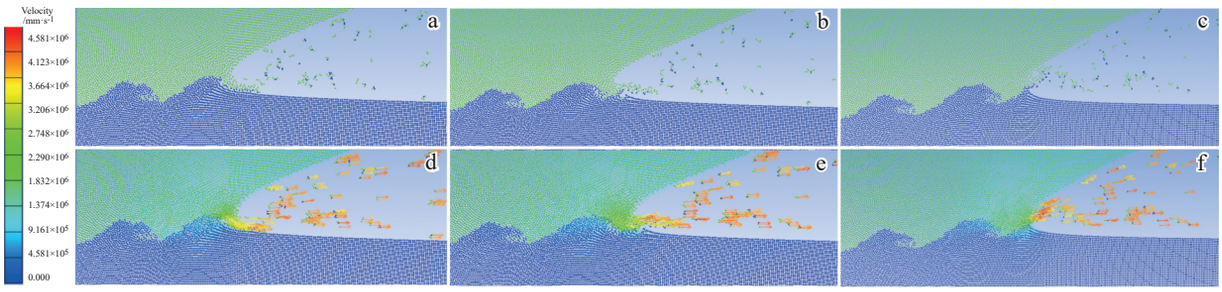

Fig.18 Jet formation (a–c) and particle velocity vector (d–f) diagrams of composite plate with flyer plate thickness of 4 mm at 4.426 μs (a, d), 4.546 μs (b, e), and 4.785 μs (c, f)

produces a jet.

Vortices are typical morphology features of waveform at the interface, which are characterized as front vortices located within the wave and rear vortices located at the shoulder of the wave. For the mechanism of vortex formation, Han et al[35] believed that the jet undergoes periodic up-and-down oscillation, leading to alternating interactions between the diverging jet and the substrate and flyer flows. When the jet deflects upward, partial jet is captured by the flyer flow to form the rear vortex; when the jet deflects downward, partial jet is captured by the substrate flow to create the front vortex.

However, extensive experiment results indicate that not all explosive welding interfaces exhibit front and rear vortices. Microstructure analysis results from the TA1/Q235 explosive welding experiments in this research cannot reveal the presence of rear vortices, either. Through numerical simulation analysis, it is found that the angle of upward deflection for the jet is restricted and does not exceed the collision angle. Thus, the jet is not captured by the flyer flow and cannot form a rear vortex.

Fig. 19 illustrates the entire growth process of a single waveform at the interface. With the movement of the collision point, the jet undergoes regulated up-and-down oscillation within a certain angular range. As shown in Fig. 19a – 19b, when the jet deflects downward, it firstly scours the surface of base plate, creating a void. This action simultaneously promotes the substrate flow, which displays fluid-like behavior, to move in the direction of the jet and to accumulate, forming a wave crest composed of substrate material. As illustrated in Fig. 19c, partial jet is captured by the substrate flow and enters the cavity, where the residual kinetic energy of the material near the cavity generates a clockwise circular motion. The velocity vector diagram of particles moving in clock-wise-circle form is shown in Fig. 20. This phenomenon leads to the intense stirring and mixing of the two materials within the vortex, resulting in the front vortex, as shown in Fig. 19d. Due to the restricted depth of the high-temperature and high-pressure zone, the thickness of the material of fluid-like behavior is also restricted. As the jet further penetrates and the wave crest grows, the jet cannot scour the substrate. It is worth noting that with the movement of the collision point, the angle of upward deflection of the jet is constrained, as shown in Fig. 19d–19e. After deflection at a certain angle, the jet quickly shifts downward to form the next cavity, as shown in Fig. 19f. Meanwhile, the jet continues to scour the substrate surface, creating a new wave crest, and this process is repeated several times. As shown in Fig. 19f, within the dashed box, the flying plate material above the waveform also exhibits a velocity vector field directed diagonally downwards to the right. This phenomenon causes the waveform to be further compressed and elongated, resulting in a rightward tilt of the waveform structure.

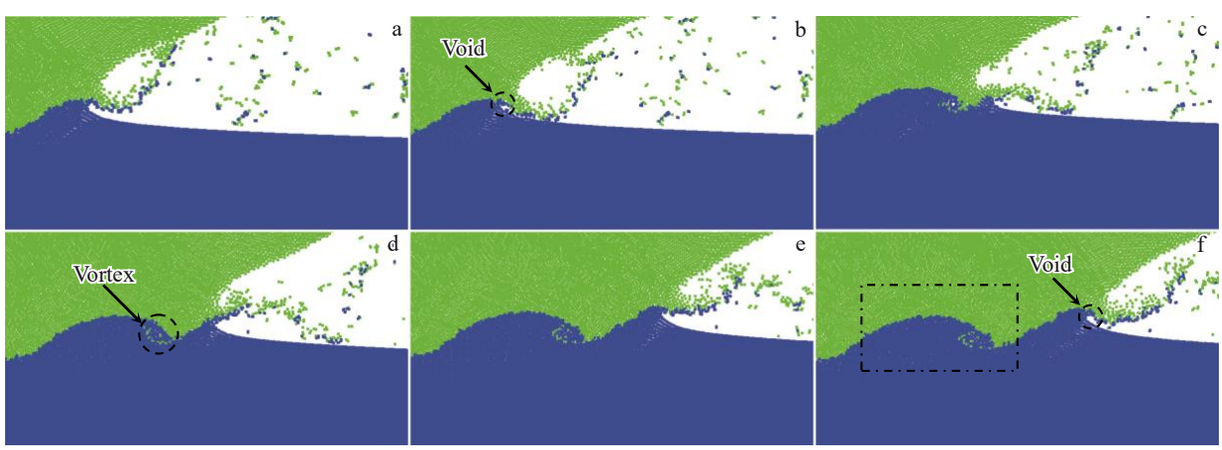

Fig.19 Schematic diagrams of single wave growth mechanism

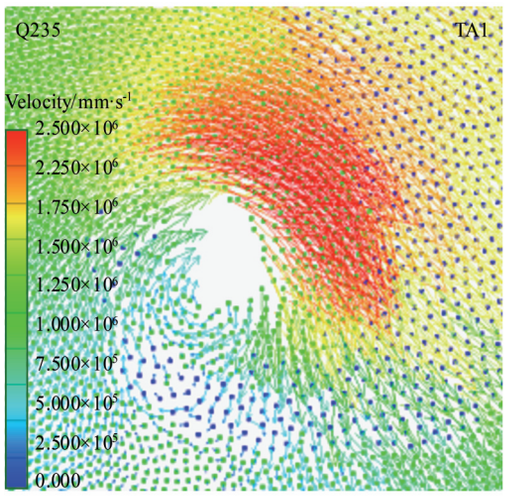

Fig.20 Velocity vector diagram of particles moving in clockwise-circle form

5 Conclusions

1) By adopting a suitable explosive detonation model to describe the motion of the flyer plate, the dynamic and static process parameters of explosive welding can be linked, thereby increasing the guiding value of numerical simulations for static process parameter experiments in explosive welding investigation.

2) The maximum bending moment caused by the detonation load on the flyer plate does not have to exceed that of the flyer plate at the dynamic yield limit. The high-quality bonding between flyer plates of varying thicknesses with base plates under the same explosive thickness can be achieved by adjusting the gap parameter.

3) The formation of the singular vortex waveform structure in the TA1/Q235 composite plate arises from the fact that the upward deflection angle of the jet does not surpass the collision angle, which prevents the jet from being captured by the flow of the flyer plate. Meanwhile, the material particles undergo intense circular motion after entering the cavity during the growth of the wavy interface.

References

1 Bai Yuliang, Liu Xuefeng, Wang Wenjing *et al*. *Chinese Journal of Engineering*[J], 2021, 43(1): 85

2 Gao Baoli, Li Pingcang, Hua Xianfeng *et al*. *Titanium Industry Progress*[J], 2005, 22(4): 36 (in Chinese)

3 Wang Ding, Sun Yunan, Xue Zhiguo *et al*. *Rare Metal Materials and Engineering*[J], 2023, 52(11): 3723

4 Yan Li. *Titanium Industry Progress*[J], 2011, 28(3): 12 (in Chinese)

5 Hu Jie, Xie Rong, Du Xunbo. *Jiangsu Ship*[J], 2016, 33(6): 6 (in Chinese)

6 Sahasrabudhe H, Harrison R, Carpenter C *et al*. *Addit Manuf*[J], 2015, 5: 1

7 Miriyev A, Stern A, Tuval E *et al*. *Journal of Materials Processing Technology*[J], 2013, 213(2): 161

8 Kim K H, Watanabe M, Mitsuishi K *et al*. *Journal of Physics D: Applied Physics*[J], 2009, 42(6): 065304

9 Lee J G, Hong S J, Lee M K *et al*. *Journal of Nuclear Materials*[J], 2009, 395(1–3): 145

10 Elrefaey A, Tillmann W. *Advanced Engineering Materials*[J], 2009, 11(7): 556

11 Li Junhan, Sun Ning, Ma Lan *et al*. *World Nonferrous Metals*[J], 2020(14): 34 (in Chinese)

12 Shi Changgen, Wang Yu, Xu Hong. *Transactions of the China Welding Institution*[J], 2012, 33(3): 109 (in Chinese)

13 Yang M, Ma H H, Shen Z W. *Journal of Materials Research and Technology*[J], 2019, 8(6): 5572

14 Kahraman N, Gülenç B, Findik F. *Journals of Materials Processing Technology*[J], 2005, 169(2): 127

15 Manikandan P, Hokamoto K, Deribas A A *et al*. *Materials Transactions*[J], 2006, 47(8): 2049

16 Wang Jian, Li Xiaojie, Dong Shouhua *et al*. *The International Journal of Advanced Manufacturing Technology*[J], 2022, 120: 6407

17 Miao Guanghong, Ma Leiming, Wu Jianqiang *et al*. *Blasting*[J], 2020, 37(2): 106 (in Chinese)

18 Zareie R H R, Akbari M S A A. *Materials Science and Engineering A*[J], 2012, 556: 454

19 Shi Changgen, Zhao Linsheng, Hou Hongbao *et al*. *Transactions of the China Welding Institution*[J], 2014, 35(5): 88 (in Chinese)

20 Ma Yong, Wang Tao, Wang Guoping *et al*. *Materials Today Communications*[J], 2023, 36: 106880

21 Bataev I A, Tanaka S, Zhou Q *et al*. *Materials & Design*[J], 2019, 169: 107649

22 Wu Xiaoming, Shi Changgen, Gao Li *et al*. *Rare Metal Materials and Engineering*[J], 2023, 52(4): 1272

23 Xu Junfeng. *Research on Evolution Mechanisms of Interfacial Meso-structures in Explosive Welded Bimetals*[D]. Hefei: University of Science and Technology of China, 2023 (in Chinese)

24 Carpenter S H, Wittman R H. *Annual Review of Materials Research*[J], 1975, 5: 177

25 Deribas A A, Zakharenko I D. *Combustion, Explosion and Shock Waves*[J], 1974, 10(3): 358

26 Zakharenko I D, Zlobin B S. *Combustion, Explosion and Shock Waves*[J], 1983, 19(5): 689

27 Wang Yuxin, Li Xiaojie, Yan Honghao *et al*. *Engineering Blasting*[J], 2018, 24(1): 1 (in Chinese)

28 Li Xiaojie, Wang Yuxin, Wang Xiaohong *et al*. *Engineering Blasting*[J], 2020, 26(5): 1 (in Chinese)

29 Koch A, Arnold N, Estermann M. *Propellants Explosives Pyrotechnics*[J], 2002, 27(6): 365

30 Shi Changgen. *The Lower Bound Theorem and Double Vertical Method of Explosive Welding*[M]. Beijing: Metallurgical

Industry Press, 2015: 94 (in Chinese)
31 Blazynski T Z. *Explosive Welding, Forming and Compaction* [M]. London: Application Science Publishers, 2012: 256
32 Yang Xueshan, Pang Lijuan, Deng Gang *et al*. *Iron Steel Vanadium Titanium*[J], 2024, 45(1): 78 (in Chinese)
33 Fronczek D M, Chulist R, Litynsk-Dobrzynska L *et al*. *Materials & Design*[J], 2017, 130: 120
34 Yang Ming, Zhang Bingyuan, Ma Honghao *et al*. *Transactions of Nonferrous Metals Society of China*[J], 2024, 34(5): 1588
35 Han Shunchang. *Phase Transformation and Fractography of the Interface of Explosive Welding*[M]. Beijing: National Defense Industry Press, 2011: 220 (in Chinese)

TA1/Q235复合板爆炸焊接数值模拟及实验

史长根，姜佳林，王海涛，罗绪川，冯　柯
(中国人民解放军陆军工程大学，江苏 南京 210007)

摘　要：为进一步降低临界装药厚度，提高爆炸焊接钛/钢复合板结合质量，在爆炸焊接下限原理指导下，采用低爆速53#药，进行了条件为复板厚度分别为1、2、4 mm，间距分别为3、6、8 mm的TA1/Q235爆炸焊接试验。计算了钛钢爆炸焊接的可焊性窗口并构建了动静态工艺参数之间的定量关系。提出了β-V_p高速倾斜碰撞模型，采用光滑粒子流体动力学方法对爆炸焊接试验进行二维数值模拟，揭示了典型波形形貌特征的生长演化机制。通过光学显微镜、扫描电子显微镜、能谱仪和电子背向散射衍射仪等微观形貌表征工具，结合剪切性能、弯曲性能、冲击韧性等力学性能测试，研究了TA1/Q235爆炸焊接复合板的界面微观组织形貌和力学性能。结果表明，界面结合质量优良，呈现典型的波形形貌，界面剪切强度平均值在330 MPa以上，冲击韧性平均值在81 J以上，试样均能实现180°弯曲且无明显的分层和裂纹等缺陷。

关键词：爆炸焊接；可焊性窗口；SPH数值模拟；微观形貌；力学性能

作者简介：史长根，男，1971年生，博士，教授，中国人民解放军陆军工程大学，江苏 南京 210007，E-mail：shichanggen71@sina.com